Correspondence

Ziv–Zakai Time-Delay Estimation Bounds for Frequency-Hopping Waveforms Under Frequency-Selective Fading

Ning Liu, Zhengyuan Xu, and Brian M. Sadler, *Fellow, IEEE*

***Abstract*—Ziv–Zakai Bayesian lower bounds on time-delay estimation (TDE) are developed for frequency hopping waveforms. These wideband waveforms are readily employed for both communications and TDE. We consider random frequency-selective fading channels, described by a Gaussian tapped delay line model with inter-hop correlation. The receiver does not know the channel realization to assist in estimating the time delay but does know the channel statistics. The development incorporates a random uniform prior on the delay. The bounds provide tight mean-square error prediction for the maximum *a posteriori* (MAP) estimator performance over a large range of signal-to-noise ratios (SNRs). They also accurately predict the TDE frequency diversity gain from multi-frequency transmission in fading channels. The special case of independent fading is discussed, including both flat Rician and Rayleigh fading, and closed-form expressions enable easy study of the effects of SNR, frequency diversity, and channel statistics on TDE.**

***Index Terms*—Frequency diversity, frequency hopping, frequency-selective fading, time-delay estimation, Ziv–Zakai bound.**

I. Introduction

Time-delay estimation (TDE) is a fundamental measurement for many practical algorithms in ranging, geolocation, synchronization, communications, and array processing. Various TDE bounds have been developed [1], and the Ziv–Zakai lower bound (ZZB) [2], [3] is among the best mean-square-error (MSE) bounds for predicting optimal estimation performance over a wide range of signal-to-noise ratios (SNRs), e.g., see [4]. The ZZB approach has also been applied to ultra-wideband signals in additive white Gaussian (AWGN) channels [5], as well as independent parallel frequency hopping and flat fading channels [6], [7]. However, in many cases, as the signal bandwidth grows we encounter a random frequency-selective fading channel [8]. An average ZZB for the case when the receiver knows the channel realization has been developed [9]. In [10], [11], a moment generating function (MGF) approach was proposed to derive a ZZB for an unknown zero-mean complex Gaussian channel with known channel statistics. A ZZB including a possible nonzero channel mean without assuming perfect channel knowledge was independently derived in [12], that reveals the TDE performance penalty associated with the lack of channel knowledge at the receiver, and this ZZB is tighter than the average ZZB.

Manuscript received December 04, 2009; accepted August 12, 2010. Date of publication August 19, 2010; date of current version November 17, 2010. The associate editor coordinating the review of this manuscript and approving it for publication was Prof. Peter Schreier. This work was supported in part by the Army Research Laboratory CTA on Communications and Networks under Grant DAAD19-01-2-0011.

N. Liu and Z. Xu are with the Department of Electrical Engineering, University of California, Riverside, CA 92521 USA (e-mail: dxu@ee.ucr.edu).

B. M. Sadler is with the Army Research Laboratory, Adelphi, MD 20783 USA (e-mail: bsadler@arl.army.mil).

Digital Object Identifier 10.1109/TSP.2010.2068547

In this correspondence, we generalize previous results [6], [7], [9], [12] to the case of unknown frequency-selective fading channels with frequency-hopping waveforms. A random Gaussian channel model is used that captures possible correlation across time and frequency. The resulting tight bound reveals achievable TDE performance for frequency-hopping waveforms that provide frequency diversity in wideband fading channels, when the receiver does not have perfect channel state information. In particular, it allows study of the choice of frequency-hopping waveform parameters, as well as the effects of channel statistics.

The derivation follows the same approach we have used [12], now with the frequency-hopping signal model as well as generalizing from a real to a complex Gaussian channel model. We first describe the signal and channel models in Section II. During the ZZB development in Section III, the log-likelihood ratio (LLR) for the associated hypothesis test is shown to follow a general quadratic form of a complex Gaussian random vector. Then the probability density function (pdf) of the LLR is obtained via an MGF approach, that in turn leads to the minimum detection error probability expression required to complete the ZZB derivation. In Section IV, the case of independent Rician and Rayleigh flat fading channels are discussed. Numerical examples in Section V show typical ZZB behaviors compared to the performance of the MAP estimator.

II. Signal and Channel Models

We consider frequency-hopping waveforms that are formed by basic pulses $p(t)$ modulated by known symbols. We will assume $p(t)$ is a square-root raised-cosine (SRRC) pulse with unit energy, symmetrically truncated to the symbol duration T_s, though the results are general. During an N-hop frequency-hopping cycle, the pulse during the ith ($i = 1, \ldots, N$) hop and kth symbol period is denoted as $p_{i,k}(t) = p(t - (i-1)MT_s - kT_s)$, where each hop has M symbols with hop dwell time MT_s. The complex envelope of the ith hop waveform is represented as

$$\begin{aligned} s_i(t) &= \sum_{k=-K_1}^{K_2} a_{i,k} p_{i,k}(t) \\ &= \sum_{k=-K_1}^{K_2} a_{i,k} p(t - (i-1)MT_s - kT_s), \\ &\qquad t \in [(i-1)MT_s, iMT_s] \end{aligned} \quad (1)$$

in which $M = K_1 + K_2 + 1$. The symbols $a_{i,k}$ can be taken from a constellation such as PSK or QAM, and we assume they are known to the receiver.

The transmitted ith hop signal $s_i(t)$ propagates through a convolutive random channel modeled as a tapped delay line with fixed spacing T_t and fading gains $\alpha_{i,l}$, given by [9], [14]

$$g_i(t) = \sum_{l=1}^{L} \alpha_{i,l} \delta(t - (l-1)T_t). \quad (2)$$

Let the L gains be in the $L \times 1$ vector $\boldsymbol{\alpha}_i$, modeled as a complex Gaussian random vector with distribution $\mathcal{CN}(\boldsymbol{\mu}_{\alpha i}, \boldsymbol{V}_i)$, where $\boldsymbol{\mu}_{\alpha i}$ is the mean vector and $\boldsymbol{V}_i$ is the covariance matrix. Further, stacking $\boldsymbol{\alpha}_i$ over N hops into vector $\boldsymbol{\alpha}$ gives a $LN \times 1$ complex Gaussian vector with mean $\boldsymbol{\mu}_\alpha$ and variance $\boldsymbol{V}$. The ith row and jth column block $\boldsymbol{V}_{ij}$ of $\boldsymbol{V}$ represents the covariance between the ith and jth hops. This

complex-valued channel model encompasses a variety of scenarios, including correlated FIR taps and subchannels of different hops.

Denote the propagation delay as t_0. For simplicity, we assume the channel delay spread is less than each hop dwell time. Extension to a much longer channel case is straightforward. Thus, due to any overlap in the time domain, there arises only inter-hop interference from the previous hop signal. The received signal for the ith hop spanning the time interval $[(i-1)MT_s, iMT_s]$ is given by

$$\begin{aligned} y_i(t) &= \sum_{l=1}^{L} \alpha_{i,l} s_i(t-(l-1)T_t - t_0) \\ &\quad + \alpha_{i-1,l} s_{i-1}(t-(l-1)T_t - t_0) + n_i(t) \\ &= \boldsymbol{\alpha}_i^T \boldsymbol{s}_i(t-t_0) + \boldsymbol{\alpha}_{i-1}^T \boldsymbol{s}_{i-1}(t-t_0) \\ &\quad + n_i(t), \quad t \in [(i-1)MT_s, iMT_s] \end{aligned} \tag{3}$$

where

$$\begin{aligned} \boldsymbol{s}_i(t-t_0) = [s_i(t-t_0), s_i(t-T_t-t_0), \ldots, \\ s_i(t-(L-1)T_t-t_0)]^T, \end{aligned} \tag{4}$$

$n_i(t)$ is complex AWGN with spectral density N_0, and we define $\boldsymbol{\alpha}_0 \triangleq \mathbf{0}$, $\boldsymbol{s}_0(t-t_0) \triangleq \mathbf{0}$ for the model to cover $y_1(t)$ in a unified form. The second term in (3) denotes the inter-hop interference from the $(i-1)$th hop to the ith hop because of the multipath propagation. The SNR of the ith hop is defined by $\mathrm{SNR}_i = \mathrm{tr}(\boldsymbol{\mu}_{\alpha i}\boldsymbol{\mu}_{\alpha i}^H + \boldsymbol{V}_i)/N_0$, where tr is the trace operator. We assume a uniform prior distribution for the propagation delay t_0 on $[0, T]$, and derive a performance bound on the estimation of t_0 next.

III. Development of the Ziv–Zakai Bound

The development of the ZZB links estimation of time delay t_0 to a hypothesis testing problem that discriminates a signal at two possible delays: hypothesis H_0 with delay a, and H_1 with delay $a+\Delta$, where $\Delta > 0$ and $a, a+\Delta \in [0, T]$ [3], [12]. Let $\hat{t}_0$ be a time-delay estimate, denote the estimation error by $\epsilon = \hat{t}_0 - t_0$, and let $P_e(a, a+\Delta)$ be the minimal probability of error achieved by the optimum detection scheme in making the hypothesis test. In general, with equally likely hypotheses, $P_e(a, a+\Delta)$ is independent of a and can be written as $P_e(\Delta)$. The TDE MSE is then lower bounded by [3]

$$\overline{\epsilon^2} \geq \frac{1}{T}\int_0^T \Delta(T-\Delta)P_e(\Delta)d\Delta. \tag{5}$$

To evaluate (5), we consider the LLR for the hypothesis test, and find $P_e(\Delta)$ using a MGF approach as in [12].

A. Received Signal Distribution

From (3), the received signal for the ith hop can be written as

$$\begin{aligned} y_i(t) = \boldsymbol{\alpha}_i^T \boldsymbol{s}_{m,i} + \boldsymbol{\alpha}_{i-1}^T \boldsymbol{s}_{m,i-1} + n_i(t), \\ t \in [(i-1)MT_s, iMT_s] \end{aligned} \tag{6}$$

where $\boldsymbol{s}_{m,i} = \boldsymbol{s}_i(t - m\Delta)$ and m takes the value 0 or 1 corresponding to hypotheses H_0 or H_1, respectively. Note that, in the context of bound development, the delay t_0 has been replaced by $m\Delta$. Collecting $y_i(t)$ and $n_i(t)$ in vectors we have

$$\begin{aligned} \boldsymbol{y}(t) = [y_1(t), \ldots, y_N(t)]^T, \quad \boldsymbol{n}(t) = [n_1(t), \ldots, n_N(t)]^T, \\ t \in [0, NMT_s]. \end{aligned}$$

From (6) and the noise independence, the distribution of $\boldsymbol{y}(t)$ conditioned on the channel gain and time delay $m\Delta$ is given by [8]

$$\begin{aligned} &p(\boldsymbol{y}(t) \,|\, \boldsymbol{\alpha}, m\Delta) \\ &= \mathcal{K} \exp \sum_{i=1}^{N} \left[-\frac{1}{N_0} \int_{(i-1)MT_s}^{iMT_s} \|y_i(t) - \boldsymbol{\alpha}_i^T \boldsymbol{s}_{m,i} - \boldsymbol{\alpha}_{i-1}^T \boldsymbol{s}_{m,i-1}\|^2 dt \right] \\ &= \mathcal{K} \exp \sum_{i=1}^{N} \Bigg\{ -\frac{1}{N_0} \int_{(i-1)MT_s}^{iMT_s} \Big[\boldsymbol{\alpha}_i^H \boldsymbol{s}_i^* \boldsymbol{s}_i^T \boldsymbol{\alpha}_i + \boldsymbol{\alpha}_{i-1}^H \boldsymbol{s}_{i-1}^* \boldsymbol{s}_{i-1}^T \boldsymbol{\alpha}_{i-1} \\ &\qquad + \boldsymbol{\alpha}_i^H \boldsymbol{s}_i^* \boldsymbol{s}_{i-1}^T \boldsymbol{\alpha}_{i-1} + \boldsymbol{\alpha}_{i-1}^H \boldsymbol{s}_{i-1}^* \boldsymbol{s}_i^T \boldsymbol{\alpha}_i \\ &\qquad - 2\mathrm{Re}\{(\boldsymbol{s}_{m,i}^* y_i(t))^H \boldsymbol{\alpha}_i\} \\ &\qquad - 2\mathrm{Re}\{(\boldsymbol{s}_{m,i-1}^* y_i(t))^H \boldsymbol{\alpha}_{i-1}\} + \|y_i(t)\|^2 \Big] dt \Bigg\} \\ &= \mathcal{K} \exp\left[-\frac{1}{N_0} \left(\boldsymbol{\alpha}^H \boldsymbol{S}_{00} \boldsymbol{\alpha} - 2\mathrm{Re}\left\{ \boldsymbol{r}_m^H \boldsymbol{\alpha} \right\} + I_y \right) \right] \end{aligned} \tag{7}$$

where $\mathcal{K}$ absorbs all the terms independent of $\boldsymbol{\alpha}_i$ and $m\Delta$, and other quantities are defined in (8), shown at the bottom of the page, with $m, m_1, m_2 \in \{0, 1\}$, and we define $y_{N+1}(t) \triangleq 0$ for the expression of $\boldsymbol{r}_{m,i}$ to cover $i = N$ as well. Note that if each subchannel is flat fading and signals from different hops do not overlap, the expression

$$\boldsymbol{S}_{m_1 m_2} \triangleq \begin{bmatrix} \boldsymbol{S}_{m_1 m_2,1,1} & \boldsymbol{S}_{m_1 m_2,1,2} & 0 & \cdots & \cdots & 0 \\ \boldsymbol{S}_{m_1 m_2,2,1} & \boldsymbol{S}_{m_1 m_2,2,2} & \boldsymbol{S}_{m_1 m_2,2,3} & \ddots & & \vdots \\ 0 & \ddots & \ddots & \ddots & \ddots & \vdots \\ \vdots & \ddots & \ddots & \ddots & \ddots & 0 \\ \vdots & & \ddots & \ddots & \ddots & \boldsymbol{S}_{m_1 m_2,N-1,N} \\ 0 & \cdots & \cdots & 0 & \boldsymbol{S}_{m_1 m_2,N,N-1} & \boldsymbol{S}_{m_1 m_2,N,N} \end{bmatrix},$$

$$\boldsymbol{S}_{m_1 m_2,i} = \boldsymbol{S}_{m_1 m_2,i,i} \triangleq \int_{(i-1)MT_s}^{(i+1)MT_s} \boldsymbol{s}_{m_1,i}^* \boldsymbol{s}_{m_2,i}^T dt,$$

$$\boldsymbol{S}_{m_1 m_2,i,i-1} \triangleq \int_{(i-1)MT_s}^{iMT_s} \boldsymbol{s}_{m_1,i}^* \boldsymbol{s}_{m_2,i-1}^T dt, \quad \boldsymbol{S}_{m_1 m_2,i-1,i} \triangleq \int_{(i-1)MT_s}^{iMT_s} \boldsymbol{s}_{m_1,i-1}^* \boldsymbol{s}_{m_2,i}^T dt,$$

$$\boldsymbol{r}_m = [\boldsymbol{r}_{m,1}^T, \ldots, \boldsymbol{r}_{m,N}^T]^T, \quad \boldsymbol{r}_{m,i} \triangleq \int_{(i-1)MT_s}^{iMT_s} \boldsymbol{s}_{m,i}^* y_i(t) dt + \int_{iMT_s}^{(i+1)MT_s} \boldsymbol{s}_{m,i}^* y_{i+1}(t) dt,$$

$$I_y = \sum_{i=1}^{N} I_{yi}, \quad I_{yi} \triangleq \int_{(i-1)MT_s}^{iMT_s} \|y_i(t)\|^2 dt, \tag{8}$$

of $\boldsymbol{S}_{m\,1,m2}$ will be block diagonal, and $\boldsymbol{r}_{m,i}$ only has the first term. We will discuss this case in detail in Section IV.

The exponent of (7) has a quadratic form in the complex Gaussian random vector $\boldsymbol{\alpha}$. We can average this over the channel $\boldsymbol{\alpha}$ using (32) from the Appendix with $s = 1$, which yields

$$\begin{aligned} &p(\boldsymbol{y}(t) \,|\, m\Delta) \\ &\quad = E_{\boldsymbol{\alpha}}[p(\boldsymbol{y}(t)|\boldsymbol{\alpha}, m\Delta)] \\ &\quad = \mathcal{K}|\boldsymbol{X}|^{-1} \exp\left\{\boldsymbol{r}_m^H \boldsymbol{W} \boldsymbol{r}_m + 2\mathrm{Re}\{\boldsymbol{h}^H \boldsymbol{r}_m\} + c\right\} \end{aligned} \tag{9}$$

where

$$\begin{aligned} &\boldsymbol{X} = \boldsymbol{I} + \frac{1}{N_0} \boldsymbol{V}^{\frac{1}{2}} \boldsymbol{S}_{00} \boldsymbol{V}^{\frac{1}{2}}, \quad \boldsymbol{W} = \frac{1}{N_0^2} \boldsymbol{V}^{\frac{1}{2}} \boldsymbol{X}^{-1} \boldsymbol{V}^{\frac{1}{2}}, \\ &\boldsymbol{h} = \frac{1}{N_0} \left(\boldsymbol{I} - \frac{1}{N_0} \boldsymbol{V}^{\frac{1}{2}} \boldsymbol{X}^{-1} \boldsymbol{V}^{\frac{1}{2}} \boldsymbol{S}_{00} \right) \boldsymbol{\mu}_\alpha = \boldsymbol{H} \boldsymbol{\mu}_\alpha, \\ &c = \boldsymbol{\mu}_\alpha^H \left(\frac{1}{N_0^2} \boldsymbol{S}_{00} \boldsymbol{V}^{\frac{1}{2}} \boldsymbol{X}^{-1} \boldsymbol{V}^{\frac{1}{2}} \boldsymbol{S}_{00} - \frac{1}{N_0} \boldsymbol{S}_{00} \right) \boldsymbol{\mu}_\alpha - \frac{I_y}{N_0}. \end{aligned}$$

B. Log-Likelihood Ratio Test

From (9), the LLR for the test of hypothesis $H_m, m = 0, 1$ is

$$\begin{aligned} \mathcal{L} &\triangleq \ln \frac{p(\boldsymbol{y}(t)|0)}{p(\boldsymbol{y}(t) \,|\, \Delta)} \\ &= \boldsymbol{r}_0^H \boldsymbol{W} \boldsymbol{r}_0 - \boldsymbol{r}_1^H \boldsymbol{W} \boldsymbol{r}_1 + 2\mathrm{Re}\{\boldsymbol{h}^H \boldsymbol{r}_0 - \boldsymbol{h}^H \boldsymbol{r}_1\} \\ &= \boldsymbol{r}^H \boldsymbol{\Psi} \boldsymbol{r} + 2\mathrm{Re}\{\boldsymbol{g}^H \boldsymbol{r}\} \\ &\underset{H_1}{\overset{H_0}{\gtrless}} 0 \end{aligned} \tag{10}$$

where

$$\boldsymbol{r} = \begin{bmatrix} \boldsymbol{r}_0 \\ \boldsymbol{r}_1 \end{bmatrix}, \quad \boldsymbol{\Psi} = \begin{bmatrix} \boldsymbol{W} & \boldsymbol{0} \\ \boldsymbol{0} & -\boldsymbol{W} \end{bmatrix}, \quad \boldsymbol{g} = \begin{bmatrix} \boldsymbol{h} \\ -\boldsymbol{h} \end{bmatrix} = \boldsymbol{G} \boldsymbol{\mu}_\alpha. \tag{11}$$

An error occurs if $\mathcal{L} < 0 \,|\, m = 0$, or if $\mathcal{L} > 0 \,|\, m = 1$. Letting $\mathcal{L}_m \triangleq \mathcal{L}|H_m$, and $\tilde{\boldsymbol{r}}_m \triangleq \boldsymbol{r}|H_m$, (10) becomes

$$\mathcal{L}_m = \tilde{\boldsymbol{r}}_m^H \boldsymbol{\Psi} \tilde{\boldsymbol{r}}_m + 2\mathrm{Re}\{\boldsymbol{g}^H \tilde{\boldsymbol{r}}_m\} \tag{12}$$

and the hypothesis test minimum error probability is

$$P_e(\Delta) = \frac{1}{2}\Pr\{\mathcal{L}_0 < 0\} + \frac{1}{2}\Pr\{\mathcal{L}_1 > 0\}. \tag{13}$$

Our goal now is to evaluate the probabilities in (13), yielding $P_e(\Delta)$ for use in the ZZB (5). First we derive the distribution of $\tilde{\boldsymbol{r}}_m$, and then use it to find the distribution of $\mathcal{L}_m$.

C. The Distribution of $\tilde{\boldsymbol{r}}_m$

Using (8) and (6) conditioned on H_0, then $\boldsymbol{r}_{m,i}$ $(m = 0, 1)$ can be expressed as

$$\begin{aligned} \boldsymbol{r}_{m,i} \,|\, H_0 &= \int_{(i-1)MT_s}^{iMT_s} \boldsymbol{s}_{m,i}^* y_i(t) + \int_{iMT_s}^{(i+1)MT_s} \boldsymbol{s}_{m,i}^* y_{i+1}(t) \\ &= \boldsymbol{S}_{m0,i,i} \boldsymbol{\alpha}_i + \boldsymbol{S}_{m0,i,i-1} \boldsymbol{\alpha}_{i-1} + \boldsymbol{S}_{m0,i,i+1} \boldsymbol{\alpha}_{i+1} + \boldsymbol{z}_{m,i} \end{aligned} \tag{14}$$

where $\boldsymbol{z}_{m,i} \triangleq \int_{(i-1)MT_s}^{(i+1)MT_s} \boldsymbol{s}_{m,i}^* [n_i(t) + n_{i+1}(t)]dt$. Stacking all N vectors $\boldsymbol{z}_{m,i}$ into a big vector $\boldsymbol{z}_m$, and similarly for $\boldsymbol{r}_{m,i} \mid H_0$, we obtain $\boldsymbol{r}_m \mid H_0 = \boldsymbol{S}_{m0} \boldsymbol{\alpha} + \boldsymbol{z}_m$. Further stacking $\boldsymbol{r}_0 \mid H_0$ and $\boldsymbol{r}_1 \mid H_0$ as in (10), we obtain

$$\tilde{\boldsymbol{r}}_0 = \boldsymbol{r} \,|\, H_0 = \boldsymbol{R}_0 \boldsymbol{\alpha} + \boldsymbol{z}, \quad \boldsymbol{R}_0 = \begin{bmatrix} \boldsymbol{S}_{00} \\ \boldsymbol{S}_{10} \end{bmatrix}, \quad \boldsymbol{z} = \begin{bmatrix} \boldsymbol{z}_0 \\ \boldsymbol{z}_1 \end{bmatrix}. \tag{15}$$

Similarly, conditioned on H_1, we find

$$\tilde{\boldsymbol{r}}_1 = \boldsymbol{r}|H_1 = \boldsymbol{R}_1 \boldsymbol{\alpha} + \boldsymbol{z}, \quad \boldsymbol{R}_1 = \begin{bmatrix} \boldsymbol{S}_{01} \\ \boldsymbol{S}_{00} \end{bmatrix}. \tag{16}$$

Therefore, under either hypothesis the data vector $\tilde{\boldsymbol{r}}_0$ or $\tilde{\boldsymbol{r}}_1$ is a linear combination of Gaussian vectors $\boldsymbol{\alpha}$ and $\boldsymbol{z}$, so that $\tilde{\boldsymbol{r}}_m$ follows a Gaussian distribution $\tilde{\boldsymbol{r}}_m \sim \mathcal{N}(\boldsymbol{\mu}_m, \boldsymbol{\Sigma}_m)$, where the mean and covariance are

$$\boldsymbol{\mu}_m = \boldsymbol{R}_m \boldsymbol{\mu}_\alpha, \quad \boldsymbol{\Sigma}_m = \left(\boldsymbol{R}_m \boldsymbol{V} \boldsymbol{R}_m^H + \boldsymbol{\Gamma} \right),$$

with

$$\boldsymbol{\Gamma} = E\{\boldsymbol{z}\boldsymbol{z}^H\} = N_0 \begin{bmatrix} \boldsymbol{S}_{00} & \boldsymbol{S}_{01} \\ \boldsymbol{S}_{10} & \boldsymbol{S}_{00} \end{bmatrix} = N_0 \begin{bmatrix} \boldsymbol{R}_0 & \boldsymbol{R}_1 \end{bmatrix}.$$

With the pdf of $\tilde{\boldsymbol{r}}_m$, each of the two probabilities $\Pr\{\mathcal{L}_0 < 0\}$ and $\Pr\{\mathcal{L}_1 > 0\}$ in (13) can be expressed as a $2LN$-dimensional integral as in [12]. However, it is computationally difficult to directly evaluate those integrals. In the next subsection we use an MGF approach [12] to find the distribution of $\mathcal{L}_m$ that results in a computationally attractive 2-dimensional integral.

D. MGF Approach

The LLR $\mathcal{L}_m$ in (12) is a quadratic form of the Gaussian vector $\tilde{\boldsymbol{r}}_m$. To find the probability distribution of $\mathcal{L}_m$, we first obtain its MGF (or characteristic function) and then apply the Fourier transform implemented efficiently using an FFT. Then, the distribution of $\mathcal{L}_m$ is used to evaluate the error probabilities in (13) via 1-dimensional integration, and the resulting $P_e(\Delta)$ is used to find the ZZB in (5).

By the definitions in (11), $\boldsymbol{g}^T \boldsymbol{\Psi}^{-1} \boldsymbol{g} = 0$. Using this, we can rewrite $\mathcal{L}_m$ in (12) as follows:

$$\mathcal{L}_m = \tilde{\boldsymbol{x}}_m^H \boldsymbol{\Psi} \tilde{\boldsymbol{x}}_m \tag{17}$$

where $\tilde{\boldsymbol{x}}_m = \tilde{\boldsymbol{r}}_m + \boldsymbol{\Psi}^{-1} \boldsymbol{g}$. Note that $\tilde{\boldsymbol{x}}_m$ is Gaussian distributed with variance $\boldsymbol{\Sigma}_m$ and mean

$$\boldsymbol{\mu}_{xm} = \boldsymbol{\mu}_m + \boldsymbol{\Psi}^{-1} \boldsymbol{g} = (\boldsymbol{R}_m + \boldsymbol{\Psi}^{-1} \boldsymbol{G}) \boldsymbol{\mu}_\alpha.$$

We introduce a zero-mean Gaussian random vector $\boldsymbol{u}_m$, obtained from $\tilde{\boldsymbol{x}}_m$ by the transformation

$$\tilde{\boldsymbol{x}}_m = \boldsymbol{\Sigma}_m^{\frac{1}{2}} \boldsymbol{P}_m \boldsymbol{u}_m + \boldsymbol{\mu}_{xm} = \boldsymbol{\Sigma}_m^{\frac{1}{2}} \boldsymbol{P}_m (\boldsymbol{u}_m + \boldsymbol{b}_m)$$

so that the variance of $\boldsymbol{u}_m$ is the identity matrix $\boldsymbol{I}$, and the vector $\boldsymbol{b}_m$ is a linear transformation of channel mean $\boldsymbol{\mu}_\alpha$ given by

$$\boldsymbol{b}_m = \boldsymbol{P}_m^H \boldsymbol{\Sigma}_m^{-\frac{1}{2}} \boldsymbol{\mu}_{xm} = \boldsymbol{P}_m^H \boldsymbol{\Sigma}_m^{-\frac{1}{2}} (\boldsymbol{R}_m + \boldsymbol{\Psi}^{-1} \boldsymbol{G}) \boldsymbol{\mu}_\alpha. \tag{18}$$

In this transformation, $\boldsymbol{P}_m$ is a unitary matrix in the eigendecomposition of the Hermitian matrix given by

$$\boldsymbol{\Sigma}_m^{\frac{1}{2}} \boldsymbol{\Psi} \boldsymbol{\Sigma}_m^{\frac{1}{2}} = \boldsymbol{P}_m \mathrm{diag}\{\lambda_1, \ldots, \lambda_{2LN}\} \boldsymbol{P}_m^H = \boldsymbol{P}_m \boldsymbol{\Lambda} \boldsymbol{P}_m^H.$$

From this, the elements u_{mk} of $\boldsymbol{u}_m$ are independent Gaussian random variables, each with zero mean and unit variance. It follows that (17) can be written as

$$\mathcal{L}_m = (\boldsymbol{u}_m + \boldsymbol{b}_m)^H \boldsymbol{\Lambda} (\boldsymbol{u}_m + \boldsymbol{b}_m) = \sum_{k=1}^{2LN} \lambda_k |u_{mk} + b_{mk}|^2 \tag{19}$$

where b_{mk} is the k-th element of $\boldsymbol{b}_m$. The MGF is obtained from (19) by applying (33) from the Appendix yielding

$$\Theta_m(s) = \prod_{k=1}^{2LN} (1 - s\lambda_k)^{-1} \exp\left\{ \frac{s\lambda_k |b_{mk}|^2}{1 - s\lambda_k} \right\}. \tag{20}$$

In (20), each of the $2LN$ product factors stems from the MGF of a scaled noncentral Chi-square random variable with one degree of freedom [15]. This observation is consistent with (19), a weighted sum of independent noncentral Chi-square random variables, where each summation term corresponds to a factor in (20).

IV. The Independent Flat Fading Case

We now discuss the ZZB when the channels are flat fading, corresponding to narrowband frequency-hopping. With $L = 1$, the channel gain α_i of the ith hop follows $\mathcal{N} \sim (\mu_{\alpha i}, V_i)$, which is Rician or Rayleigh flat fading. Then the dimension of the total channel covariance matrix $\boldsymbol{V}$ reduces to $N \times N$, in which V_{ij} is determined by V_i, V_j and the channel correlation coefficient between the two hops. Also the channel mean vector reduces to $\boldsymbol{\mu}_\alpha = [\mu_{\alpha 1}, \ldots, \mu_{\alpha N}]^T$.

The flat fading channel has no memory and so there will be no overlap between hops in the time domain. So the inter-hop interference terms disappear in the signal and distribution expressions. The received signal in (6) becomes

$$y_i(t) = \alpha_i s_{m,i} + n_i(t), \quad t \in [(i-1)MT_s, iMT_s] \tag{21}$$

and the quantities in (7) reduce to

$$\begin{aligned} \boldsymbol{S}_{m1m2} &= \mathrm{diag}\{S_{m1m2,1,1}, \ldots, S_{m1m2,N,N}\}, \\ r_{m,i} &= \int_{(i-1)MT_s}^{iMT_s} s^*_{m,i} y_i(t) dt. \end{aligned} \tag{22}$$

Moreover, we assume the channel α_i over each hop is independent and identical distributed (i.i.d), and then the signal correlation $S_{m1m2,i}$ is the same for each hop. By this assumption, $\boldsymbol{V}$ becomes diagonal. The joint distribution of the received signal over independent flat fading channels becomes

$$\begin{aligned} p(\boldsymbol{y}(t) \mid m\Delta) &= \prod_{i=1}^{N} p(y_i(t) | m\Delta) \\ &\propto \prod_{i=1}^{N} \exp\left\{ W_i r_{m,i}^2 + 2\mathrm{Re}\{h_i^* r_{m,i}\} \right\} \end{aligned} \tag{23}$$

where

$$\begin{aligned} W_i &= \frac{V_i}{N_0(N_0 + V_i S_{00,i})} \\ h_i &= \frac{\mu_i}{N_0 + V_i S_{00,i}}, \quad S_{00,i} \triangleq S_{00,i,i}. \end{aligned}$$

In this case, the LLR is

$$\begin{aligned} \mathcal{L} &= \boldsymbol{r}^H \boldsymbol{\Psi} \boldsymbol{r} + 2\mathrm{Re}\{\boldsymbol{g}^H \boldsymbol{r}\} \\ &= \sum_{i=1}^{N} W_i \left(r_{0,i}^2 - r_{1,i}^2 \right) + 2\mathrm{Re}\{h_i^* (r_{0,i} - r_{1,i})\}. \end{aligned} \tag{24}$$

This is the sum of the LLRs corresponding to each subchannel. Accumulation helps to improve the decision performance in fading and noise, a benefit of frequency hopping diversity.

Conditioned on hypothesis H_m, the mean and variance of $\tilde{\boldsymbol{r}}_{m,i} \triangleq [r_{0,i} \mid H_m \; r_{1,i} | H_m]^T$ are given by (25) and (26), shown at the bottom of the page. Next, we consider the Rician (line-of-sight) and Rayleigh (non-line-of-sight) cases.

A. Rician Fading Case

Under the i.i.d condition, we have the same W_i and h_i for each i, and $\tilde{\boldsymbol{r}}_{m,i}$ is also i.i.d. Then with $W_i > 0$, the error probability $P_e(\Delta)$ becomes

$$\begin{aligned} P_e(\Delta) = \Pr\{\mathcal{L}_0 < 0\} = \Pr\Bigg\{ \sum_{i=1}^{N} \Bigg[\left| r_{0,i} | H_0 + \frac{h_i}{W_i} \right|^2 \\ - \left| r_{1,i} | H_0 + \frac{h_i}{W_i} \right|^2 \Bigg] < 0 \Bigg\}. \end{aligned} \tag{27}$$

Denote the Gaussian variables within the brackets as $A = r_{0,i}|H_0 + h_i/W_i$ and $B = r_{1,i}|H_0 + h_i/W_i$, where $r_{0,i}|H_0$ and $r_{1,i}|H_0$ are elements of $\tilde{\boldsymbol{r}}_{0,i}$. For these two variables, mean μ_A, μ_B, variance Σ_A, Σ_B and covariance Σ_{AB} can be found from (25) as

$$[\mu_A, \mu_B]^T = \boldsymbol{\mu}_{i,0} + \frac{h_i}{W_i}[1,1]^T, \quad \boldsymbol{\Sigma}_{i,0} = \begin{bmatrix} \Sigma_A & \Sigma_{AB} \\ \Sigma_{AB}^* & \Sigma_B \end{bmatrix}.$$

Thus from the results in [8, pp. 619–624, (9A.11)] or [16, pp. 882–886, (B-21)], a closed form for $P_e(\Delta)$ can be obtained:

$$\begin{aligned} P_e(\Delta) &= Q_1(a,b) \\ &\quad - \left[1 - \frac{\sum_{i=0}^{N-1} \binom{2N-1}{i} \eta^i}{(1+\eta)^{2N-1}} \right] \exp\left(-\frac{a^2+b^2}{2} \right) I_0(ab) \\ &\quad + \frac{1}{(1+\eta)^{2N-1}} \Bigg\{ \sum_{i=2}^{N} \binom{2N-1}{N-i} \{ \eta^{N-i} [Q_i(a,b) - Q_1(a,b)] \\ &\quad - \eta^{N-1+i} [Q_i(b,a) - Q_1(b,a)] \} \Bigg\} \end{aligned} \tag{28}$$

in which

$$\begin{aligned} a &= \left[\frac{2v_1^2 v_2 (\xi_1 v_2 - \xi_2)}{(v_1 + v_2)^2} \right]^{1/2} \\ b &= \left[\frac{2v_1^2 v_2 (\xi_1 v_1 + \xi_2)}{(v_1 + v_2)^2} \right]^{1/2} \\ \eta &= v_2 / v_1, \\ v_{\frac{1}{2}} &= \sqrt{w^2 + \frac{1}{\Sigma_A \Sigma_B - |\Sigma_{AB}|^2}} \mp w \\ w &= \frac{\Sigma_A - \Sigma_B}{2(\Sigma_A \Sigma_B - |\Sigma_{AB}|^2)} \\ \xi_1 &= N(|\mu_A|^2 \Sigma_B + |\mu_B|^2 \Sigma_A - \mu_A^* \mu_B \Sigma_{AB} \\ &\quad - \mu_A \mu_B^* \Sigma_{AB}^*), \quad \xi_2 = N(|\mu_A|^2 + |\mu_B|^2). \end{aligned}$$

$$H_0: \quad \boldsymbol{\mu}_{0,i} = \begin{bmatrix} S_{00,i}\mu_{\alpha i} \\ S_{10,i}\mu_{\alpha i} \end{bmatrix}, \quad \boldsymbol{\Sigma}_{0,i} = \begin{bmatrix} S_{00,i}^2 V_i + N_0 S_{00,i} & S_{00,i} S_{10,i}^* V_i + N_0 S_{10,i}^* \\ S_{00,i} S_{10,i} V_i + N_0 S_{10,i} & |S_{10,i}|^2 V_i + N_0 S_{00,i} \end{bmatrix} \tag{25}$$

$$H_1: \quad \boldsymbol{\mu}_{1,i} = \begin{bmatrix} S_{10,i}^*\mu_{\alpha i} \\ S_{00,i}\mu_{\alpha i} \end{bmatrix}, \quad \boldsymbol{\Sigma}_{1,i} = \begin{bmatrix} |S_{10,i}|^2 V_i + N_0 S_{00,i} & S_{00,i} S_{10,i}^* V_i + N_0 S_{10,i}^* \\ S_{00,i} S_{10,i} V_i + N_0 S_{10,i} & S_{00,i}^2 V_i + N_0 S_{00,i} \end{bmatrix}. \tag{26}$$

B. Rayleigh Fading Case

For the Rayleigh fading case as studied in [6], $\mu_i = 0$ and so $h_i = 0$. The LLR becomes $\mathcal{L} = \sum_{i=1}^{N}(|r_{0,i}|^2 - |r_{1,i}|^2)$, and the test reduces to the comparison of the signal power $|r_{0,i}|^2$ with $|r_{1,i}|^2$. The error probability expression (27) matches (113) in [6], and $\boldsymbol{\mu}_{i,0} = [0,0]^T$ and $\boldsymbol{\Sigma}_{i,0}$ in (25) matches distribution parameters of (115) in [6]. Therefore, the same closed-form expression for error probability $P_e(\Delta)$ as in [6, (116) and (117)] follows:

$$P_e(\Delta) = \sum_{i=0}^{N-1} \binom{2N-1}{i} \left(\frac{1+\nu(\Delta)}{2}\right)^i \left(\frac{1-\nu(\Delta)}{2}\right)^{2N-1-i} \tag{29}$$

with

$$\nu(\Delta) = \left[1 + \frac{4(1+\mathrm{SNR}_i \cdot S_{00,i})}{(S_{00,i}\cdot \mathrm{SNR}_i)^2 \cdot [1 - |S_{10,i}/S_{00,i}|^2]}\right]^{-1/2}.$$

Each summation term in (29) is a binomial distribution $f(i; 2N-1, (1+\nu(\Delta)/2))$. When the number of hops N is large, it can be approximated by a Gaussian distribution for simplified evaluation [18]. Moreover, $\nu(\Delta)$ is close to 1 in the high SNR region and then P_e is dominated by the last several summation terms with large i. Selecting the last U summation terms, P_e can be approximated as

$$\begin{aligned} P_e(\Delta) &\approx \sum_{i=N-U}^{N-1} \binom{2N-1}{i} \left(\frac{1+\nu(\Delta)}{2}\right)^i \left(\frac{1-\nu(\Delta)}{2}\right)^{2N-1-i} \\ &\approx \sum_{i=N-U}^{N-1} \frac{\exp\left\{-\frac{[i-(2N-1)(1+\nu(\Delta))/2]^2}{(2N-1)(1-\nu^2(\Delta))/2}\right\}}{\sqrt{2\pi(2N-1)(1-\nu^2(\Delta))/4}}. \end{aligned} \tag{30}$$

For large N, it suffices to choose a small U. This approximate expression shows the effect of frequency hopping diversity (in terms of N) on P_e, and therefore on the ZZB. We will show numerically how the ZZB decreases with increasing N.

V. Numerical Examples

We adopt the root MSE (RMSE) of the TDE as the performance metric, and use both the MGF approach in Section III-D and the closed-form expressions in Sections IV-A and IV-B to evaluate the ZZB. Unless otherwise specified, $p(t)$ is a normalized square-root raised cosine (SRRC) pulse with roll-off factor $\beta = 0$ and mean-square bandwidth $B = 1/12$. We consider the SRRC pulse due to its common use in communications systems, and its good spectral occupancy properties. We note that a rectangular pulse can produce better TDE results, but at the cost of more spectral occupancy (see the results in [12]). We symmetrically truncate the SRRC to duration $T_s = 12$, i.e., 12 times beyond the first zero-crossing point. The channel has tap spacing $T_t = 1$ and $L = 5$ taps. Note that we normalize time to T_t. The time delay has a uniform prior over $[0, 30]$; i.e., $T = 30$. The transmission duration is NMT_s, which is a cycle of N hops, where the number of transmitted symbols per hop is set to $M = 80/N$. As the transmitted pulse has unit energy, and the number of symbols in one cycle is fixed to $MN = 80$, the total transmitted energy for one-shot TDE is fixed and independent of the number of hops N. We assume the hops are equally spaced, and the center frequency separation of neighboring hops is set to $\Delta f = 1$. Then, the ith and jth hops are separated by $|i-j|\Delta f$.

The channel fading distribution of $\boldsymbol{\alpha}_i$ and SNR_i are the same for each hop. To obtain the covariance between the pth and qth channel taps ($p, q = 1, \ldots, LN$), we need to compute both the variance of each channel tap, and the correlation coefficients between them. To compute the variance and power of the taps, the mean $\boldsymbol{\mu}_{\alpha i}$ and the variance or power $\boldsymbol{V}_i$ for all the channel taps in the ith hop are generated using the exponential power decay profile given in [9], with the mean of the first tap obtained from a Rician-K factor, and all other taps with zero mean. The frequency-hopping channel correlation coefficient between the pth and qth channel taps from the ith and jth hops, respectively, is expressed as $\rho_{p,q} = \rho^t_{p,q}(1+\sqrt{-1}\sigma 2\pi|i-j|\Delta f)/(1+(\sigma 2\pi|i-j|\Delta f)^2)$, which is developed in [13] following the classical Jakes model [14, pp. 46–51]. The temporal correlation $\rho^t_{p,q}$ depends on the time separation between the pth and qth taps. In the following numerical examples $\rho^t = 0.8$ is adopted for the first two neighboring taps, and $\sigma = 1$ is the root-mean-square value of the delay spread.

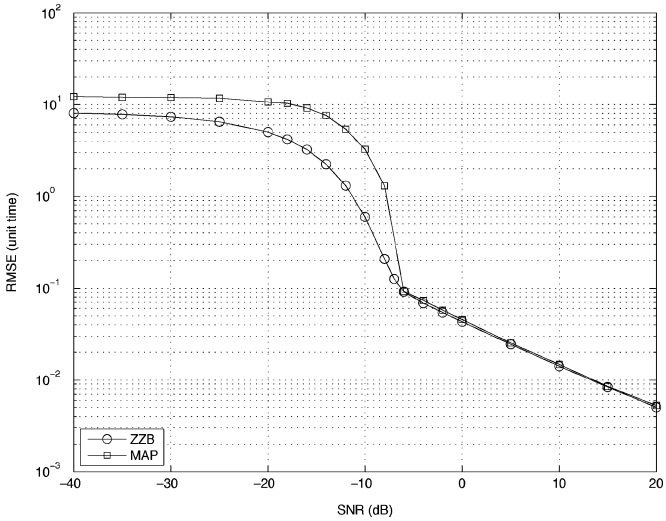

Fig. 1. Time-delay estimation results, comparing the ZZB and the corresponding MAP estimation performance. $N = 4$ hops, $M = 20$ symbols, and an FIR random channel, with first tap Rician-$K = 20$ dB, and later taps Rayleigh distributed.

Fig. 1 plots the ZZB for a frequency-hopping waveform with $N = 4$ hops in comparison with the performance of the optimum MAP estimator. The MAP estimator is implemented by using (9) as follows (see also [12, eq. (78)]):

$$\hat{t}_{0,\mathrm{MAP}} = \arg\max_{t_0}\left\{\frac{1}{T}\exp\left(\boldsymbol{r}^H_{t_0}\boldsymbol{W}\boldsymbol{r}_{t_0} + 2\mathrm{Re}\{\boldsymbol{h}^H\boldsymbol{r}_{t_0}\}\right)\right\} \tag{31}$$

where $1/T$ is the prior on delay t_0, and $\boldsymbol{r}_{t_0}$ is defined by replacing $m\Delta$ with t_0 in $\boldsymbol{r}_m$. The channel Rician-K factor is set to $K = 20$ dB. The ZZB predicts typical behavior for TDE. At low SNR, the ZZB converges to $T/\sqrt{12}$, similar to other cases [9], [12]. High SNR threshold occurs at about -6 dB, below which TDE performance rapidly degrades. Above the high SNR threshold, the ZZB decreases linearly with increasing SNR, with a slope of about -0.5, similar to bandwidth limited pulse cases studied by Ziv and Zakai [2], [3]. Moreover, the ZZBs track the MAP estimator threshold behavior and the MAP RMSE converges to the ZZB at high SNR as expected. At low SNR, the MAP RMSE converges to $T/\sqrt{6}$, higher than the ZZB's convergence level. The gap has been quantitatively analyzed in [12], and occurs due to approximations in the derivation of the original ZZB inequality by Ziv and Zakai.

The closed-form expressions of the ZZB in (28) and (29) for independent flat fading channels have much lower numerical complexity than the MGF approach, and are useful for quickly testing parameter effects on the ZZB. Fig. 2 compares the ZZBs at various number of hops, $N = 1, 2, 4, 8$, and 16, under the independent flat Rayleigh fading channel discussed in Section IV-B. The ZZB without the Gaussian approximation in (29), and with the Gaussian approximation in (30), are

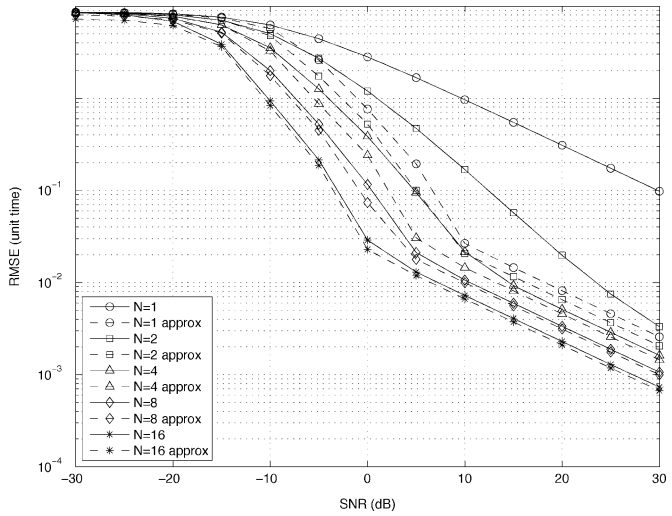

Fig. 2. ZZBs with independent flat Rayleigh channels show the frequency hopping diversity gain, with curves parameterized by the number of hops $N = 1, 2, 4, 8$, and 16.

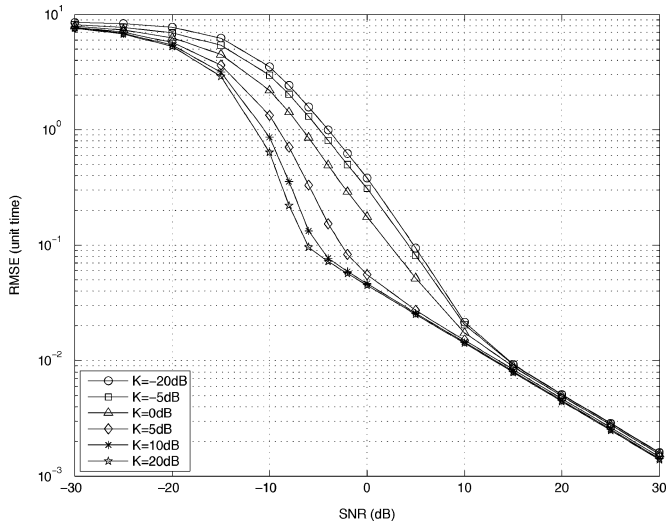

Fig. 3. ZZBs for varying Rician-K factor, with independent flat fading channels. The stronger Rician channel yields significant TDE performance gain in the mid-SNR range.

plotted with $U = 3$ for $N > 2$, and $U = N$ when $N \leq 2$. As can be seen, larger N leads to lower RMSE level and the high SNR threshold occurs at lower SNR, about 25, 14, 5, and 0 dB for $N = 2$, 4, 8 and 16, respectively. Recalling that the total transmitted energy is fixed and independent of N, the RMSE reduction arises solely from the frequency-hopping diversity available via hopping through different channel realizations. This comparison clearly exemplifies the frequency diversity effect on TDE. The diversity gain from increasing N over 2 to 16 achieves a maximum of about 18 dB at RMSE of 2×10^{-2}, with a constant gain of about 12 dB in the high SNR regime.

In Fig. 3, we use (28) to evaluate the effect of Rician-K factor on the ZZB under independent flat Rician fading. The FH transmission has $N = 4$ hops and K varies from -20 to 20 dB. The ZZBs exhibit the most difference in the moderate SNR region over -10 to 5 dB, and the maximum difference is about 11 dB at RMSE 10^{-1}. In this region, the ambiguities in signal correlation dominate the TDE error, which occur due to fading. In the high SNR region, the effects of varying K are minimized and the bounds for different K coincide.

VI. Conclusion

In this correspondence, we developed a Bayesian bound on time-delay estimation using the Ziv–Zakai approach, for frequency hopping waveforms. The development incorporated both frequency-selective fading channels and possible correlation among FIR channel taps as well as frequency-hopping subchannels. Comparison with the MAP estimator indicates that the ZZB is tight for the useful SNR range. Closed-form ZZB expressions were obtained for independent flat fading channels, enabling study of system parameter effects. The bound shows the benefit of frequency diversity in frequency-selective fading channels through frequency-hopping transmission. Other multiple-carrier signaling schemes that use multiple frequencies for transmission, such as orthogonal frequency-division multiplexing (OFDM), are expected to provide similar diversity gain for TDE and are of interest for future work.

Appendix I
MGF of a Quadratic Function of a Complex Gaussian Random Vector

Assume $\boldsymbol{r}$ is a complex Gaussian vector with distribution $p(\boldsymbol{r})$ denoted by $\boldsymbol{r} \sim \mathcal{N}(\boldsymbol{\mu}, \boldsymbol{\Sigma})$. For Hermitian symmetric matrix $\boldsymbol{\Psi}$, complex vector $\boldsymbol{g}$ and real scalar d, the MGF of $Q = \boldsymbol{r}^H \boldsymbol{\Psi} \boldsymbol{r} + 2\mathrm{Re}\{\boldsymbol{g}^H \boldsymbol{r}\} + d$ is defined as $\Theta(s) = E\{\exp(sQ)\}$. Using the same integration technique as shown in [17] for the quadratic form $\boldsymbol{r}^H \boldsymbol{\Psi} \boldsymbol{r}$, and after a similar manipulation as [15, Theorem 3.2a.1], we can obtain a symmetric form of the MGF given by

$$\begin{aligned}\Theta(s) = {} & |\boldsymbol{I} - s\boldsymbol{\Sigma}^{\frac{1}{2}} \boldsymbol{\Psi} \boldsymbol{\Sigma}^{\frac{1}{2}}|^{-1} \\ & \times \exp\left\{ s\left(\boldsymbol{\mu}^H \boldsymbol{\Psi} \boldsymbol{\mu} + \mathrm{Re}\{\boldsymbol{g}^H \boldsymbol{\mu}\} + d\right) \right. \\ & + s^2 \left(\boldsymbol{\Sigma}^{\frac{1}{2}} \boldsymbol{g} + \boldsymbol{\Sigma}^{\frac{1}{2}} \boldsymbol{\Psi} \boldsymbol{\mu}\right)^H (\boldsymbol{I} - s\boldsymbol{\Sigma}^{\frac{1}{2}} \boldsymbol{\Psi} \boldsymbol{\Sigma}^{\frac{1}{2}})^{-1} \\ & \left. \times \left(\boldsymbol{\Sigma}^{\frac{1}{2}} \boldsymbol{g} + \boldsymbol{\Sigma}^{\frac{1}{2}} \boldsymbol{\Psi} \boldsymbol{\mu}\right) \right\}. \end{aligned} \tag{32}$$

If $\boldsymbol{g} = 0$ and $d = 0$, then Q shrinks to $Q = \boldsymbol{r}^H \boldsymbol{\Psi} \boldsymbol{r}$. Then, $\Theta(s)$ can be found as

$$\begin{aligned}\Theta(s) = {} & \left|\boldsymbol{I} - s\boldsymbol{\Sigma}^{\frac{1}{2}} \boldsymbol{\Psi} \boldsymbol{\Sigma}^{\frac{1}{2}}\right|^{-1} \exp\left\{ s\boldsymbol{\mu}^H \boldsymbol{\Sigma}^{-\frac{1}{2}} \left(\boldsymbol{\Sigma}^{\frac{1}{2}} \boldsymbol{\Psi} \boldsymbol{\Sigma}^{\frac{1}{2}}\right) \right. \\ & \left. \times \left(\boldsymbol{I} - s\boldsymbol{\Sigma}^{\frac{1}{2}} \boldsymbol{\Psi} \boldsymbol{\Sigma}^{\frac{1}{2}}\right)^{-1} \boldsymbol{\Sigma}^{-\frac{1}{2}} \boldsymbol{\mu} \right\}. \end{aligned} \tag{33}$$

References

[1] B. M. Sadler and R. J. Kozick, "A survey of time delay estimation performance bounds," in *Proc. 4th IEEE Workshop Sensor Array Multichannel Signal Processing (Invited Paper)*, Jul. 2006, pp. 282–288.

[2] J. Ziv and M. Zakai, "Some lower bounds on signal parameter estimation," *IEEE Trans. Inf. Theory*, vol. IT-15, no. 3, pp. 386–391, May 1969.

[3] D. Chazan, M. Zakai, and J. Ziv, "Improved lower bounds on signal parameter estimation," *IEEE Trans. Inf. Theory*, vol. 21, no. 1, pp. 90–93, Jan. 1975.

[4] H. L. van Trees and K. L. Bell, *Bayesian Bounds for Parameter Estimation and Nonlinear Filtering/Tracking*. New York: IEEE Press, 2007.

[5] B. M. Sadler, L. Huang, and Z. Xu, "Ziv–Zakai time delay estimation bound for ultra-wideband signals," presented at the IEEE Int. Conf. Acoustics, Speech, Signal Processing (ICASSP), Honolulu, HI, Apr. 15–20, 2007.

[6] R. J. Kozick and B. M. Sadler, "Communication channel estimation and waveform design: Time delay estimation on parallel, flat fading channels," Army Research Lab., Adelphi, MD, Tech. Rep. ARL-TR-5046, Feb. 2010.

[7] R. J. Kozick and B. M. Sadler, "Bounds and algorithms for time delay estimation on parallel, flat fading channels," in *Proc. IEEE Int. Conf. Acoustics, Speech, Signal Processing (ICASSP)*, Apr. 2008, pp. 2413–2416.

[8] M. K. Simon and M.-S. Alouini, *Digital Communication Over Fading Channels: A Unified Approach to Performance Analysis*, 2nd ed. New York: Wiley, 2005.
[9] Z. Xu and B. M. Sadler, "Time delay estimation bounds in convolutive random channels," *IEEE J. Sel. Topics Signal Process. (Special Issue on Performance Limits of Ultra-Wideband Systems)*, vol. 1, no. 3, pp. 418–430, Oct. 2007.
[10] H. Anouar, A. M. Hayar, R. Knopp, and C. Bonnet, "Ziv–Zakai lower bound on the time delay estimation of UWB signals," presented at the 2nd IEEE-EURASIP Int. Symp. Control, Commun., Signal Proc., Marrakech, Morocco, Mar. 13–15, 2006.
[11] H. Anouar, A. M. Hayar, R. Knopp, and C. Bonnet, "Lower bound on time-delay estimation error of UWB signals," presented at the Asilomar Conf. Signals, Systems, Computers, Pacific Grove, CA, Nov. 4–7, 2007.
[12] B. M. Sadler, N. Liu, and Z. Xu, "Ziv–Zakai bounds on time delay estimation in unknown convolutive random channels," *IEEE Trans. Signal Process.*, vol. 58, no. 5, pp. 2729–2745, May 2010.
[13] M. Pätzold, F. Laue, and U. Killat, "A frequency hopping Rayleigh fading channel simulator with given correlation properties," presented at the IEEE Int. Workshop Intelligent Signal Processing Communication Systems (ISPACS), Kuala Lumpur, Malaysia, Nov. 1997.
[14] W. C. Jakes, Jr., *Microwave Mobile Communications*. New York: Wiley, 1974.
[15] A. M. Mathai and S. B. Provost, *Quadratic Forms in Random Variables: Theory and Applications*. New York: Marcel Dekker, 1992.
[16] J. G. Proakis, *Digital Communications*, 4th ed. New York: McGraw-Hill, 2001.
[17] G. L. Turin, "The characteristic function of Hermitian quadratic forms in complex normal variables," *Biometrika*, vol. 47, no. 1/2, pp. 199–201, Jun. 1960.
[18] A. Papoulis and S. U. Pillai, *Probability, Random Variables and Stochastic Processes*, 4th ed. New York: McGraw-Hill, 2002.

On the Fractional Linear Scale Invariant Systems

Manuel Duarte Ortigueira

***Abstract*—The linear scale invariant systems are introduced for both integer and fractional orders. They are defined by the generalized Euler–Cauchy differential equation. The quantum fractional derivatives are suitable for dealing with this kind of systems, allowing us to define impulse response and transfer function with the help of the Mellin transform. It is shown how to compute the impulse responses corresponding to the two half plane regions of convergence of the transfer function.**

***Index Terms*—Fractional linear systems, fractional quantum derivative, linear scale invariant systems.**

I. Introduction

Braccini and Gambardella introduced the concept of "form-invariant" filters [5]. These are systems such that a scaling of the input gives rise to a scaling of the output. This is important in detection and estimation of signals with unknown size requiring some type of pre-processing: for example edge sharpening in image processing or in radar signals. However in their attempt to define such systems, they did not give any formulation in terms of a differential equation. The linear scale invariant systems (LSIS) were really introduced by Yazici and Kashyap [15] for analysis and modelling 1/f phenomena and in general the self-similar processes, namely the scale stationary processes. Their approach was based on an integer order Euler–Cauchy differential equation. However, they solved only a particular case corresponding to the all pole case. To insert a fractional behavior, they proposed the concept of pseudo-impulse response. Here we avoid this procedure by presenting a fractional derivative based general formulation of the LSIS. These are described by fractional Euler–Cauchy equations [12]. The fractional quantum derivatives [11]–[14] are suitable for dealing with these systems. The use of the Mellin transform allowed us to define the multiplicative convolution and, from it, it is shown that the power function is the eigenfunction of the LSIS and the eigenvalue is the transfer function.

The computation of the impulse response from the transfer function is done following a procedure very similar to the used in the shift-invariant systems [9], [10]. This is done into two steps. In the first, we solve a particular case with integer differentiation orders. Later, we solve for the fractional case.

The correspondence outlines as follows. The general Euler–Cauchy equation is introduced in Section II, where we define impulse response and transfer function of the systems represented by such equation. The fractional quantum derivatives important tools in this study are also presented. In Section III, we perform the impulse response computations for the uniform order case. In the Appendix, we present the two derivatives and their integral formulations. Finally, we will present some conclusions.

II. The General Formulation

A. The Fractional Quantum Derivative

We are going to consider a general formulation for the LSIS. The integer order case was studied in [15]. To do it, we need to introduce the two fractional quantum derivatives that we proposed before [11]–[13]. As in [13], we will call "below t" (analog to anti-causal) and "above t" (analog to causal) derivatives. This means that we have two different ways of performing limit computations that do not lead necessarily to the same result. Working in the context of the Mellin transform, we obtain two different regions of convergence: left and right relatively to a vertical straight line. This is not needed when dealing with integer order systems [15] because we only have one Mellin transform for $t^n f^{(n)}(t)$ if n is integer. The two fractional quantum derivatives are given by [11]–[13]

$$D_q^\alpha f(t) = \lim_{q\to 1} \frac{\sum_{j=0}^{\infty} \begin{bmatrix} \alpha \\ j \end{bmatrix}_q (-1)^j q^{j(j+1)/2} q^{-j\alpha} f(q^j t)}{(1-q)^\alpha t^\alpha} \tag{1}$$

and

$$D_{q^{-1}}^\alpha f(t) = \lim_{q\to 1} \frac{\sum_{j=0}^{\infty} \begin{bmatrix} \alpha \\ j \end{bmatrix}_q (-1)^j q^{j(j-1)/2} f(q^{-j} t)}{(1-q^{-1})^\alpha t^\alpha} \tag{2}$$

where $0 < q < 1$. When α is a positive integer, these derivatives give the result we usually obtain and lead to the results obtained by Yazici and Kashyap [15]. It is interesting to remark that in (1) we are using left values ("below t"), while in (2) we use right values ("above t"). If

Manuscript received February 25, 2010; accepted September 08, 2010. Date of publication September 20, 2010; date of current version November 17, 2010. This work was supported by the Portuguese Foundation for Science and Technology through the program FEDER/POSC and the FCT (CTS multiannual funding) through the PIDDAC Program funds.

The author is with the UNINOVA and Department of Electrical Engineering of Faculdade de Ciências e Tecnologia da UNL, Campus da FCT da UNL, Quinta da Torre, 2825 –114 Monte da Caparica, Portugal, and also with the INESC-ID, 1000-029 Lisboa, Portugal (e-mail: mdortigueira@uninova.pt, mdo@fct.unl.pt).

Color versions of one or more of the figures in this correspondence are available online at http://ieeexplore.ieee.org.

Digital Object Identifier 10.1109/TSP.2010.2077633